

## Supporting Information

### Coherent TiO<sub>2</sub>/BaTiO<sub>3</sub> heterostructure as a functional reservoir and promoter for polysulfide intermediates

Hong-En Wang <sup>a</sup>, Kaili Yin <sup>a</sup>, Xu Zhao <sup>d</sup>, Ning Qin <sup>b</sup>, Yu Li <sup>a</sup>, Zhao Deng <sup>a,\*</sup>, Liuchun Zheng <sup>c,\*</sup>, Bao-Lian Su <sup>a,e</sup>, Zhouguang Lu <sup>b,\*</sup>

<sup>a</sup> State Key Laboratory of Advanced Technology for Materials Synthesis and Processing, Wuhan University of Technology, Wuhan 430070, China. E-mail: [dengzhao@whut.edu.cn](mailto:dengzhao@whut.edu.cn)

<sup>b</sup> Department of Materials Science and Engineering, Southern University of Science and Technology of China, Shenzhen, China. Email: [luzg@sustc.edu.cn](mailto:luzg@sustc.edu.cn)

<sup>c</sup> Key Laboratory of Engineering Plastics, Institute of Chemistry, Chinese Academy of Sciences (ICCAS), Beijing 100190, P. R. China. Email: [hubeizlc@iccas.ac.cn](mailto:hubeizlc@iccas.ac.cn)

<sup>d</sup> School of Materials Science and Engineering, Harbin Institute of Technology, Harbin 150001, China.

<sup>e</sup> Laboratory of Inorganic Materials Chemistry (CMI), University of Namur, 61 rue de Bruxelles, B-5000 Namur, Belgium.

## **Experimental.**

### **Materials synthesis.**

All chemicals were analytically pure grade and used as received.

***Synthesis of TiO<sub>2</sub>/oleylamine (OA) precursor.*** The TiO<sub>2</sub>/OA precursor was prepared by a facile sol-gel process. In a typical procedure, tetrabutyl titanate (4.5 mL) was rapidly added into 200 mL of ethanol containing oleylamine (1.8 mL) and H<sub>2</sub>O (0.8 mL) under strong stirring at room temperature. The resultant white precipitates were kept static at room temperature overnight, then collected by centrifugation and rinsed with ethanol three times and finally dried at 80 °C in air.

***Synthesis of porous TiO<sub>2</sub>.*** The porous TiO<sub>2</sub> was synthesized by hydrothermal treatment of TiO<sub>2</sub>/OA precursor (0.2 g) in a mixture of 20 mL H<sub>2</sub>O and 40 mL ethanol in a sealed PTFE-lined autoclave at 160 °C for 12 h. The obtained product was thoroughly rinsed with ethanol and deionized H<sub>2</sub>O, followed by drying at 60 °C in air. Then, the dried product was annealed at 500 °C in air for 2 h to remove the residual organics at particle surface.

***Synthesis of porous TiO<sub>2</sub>/BaTiO<sub>3</sub> heterojunction.*** Typically, 0.2 g porous TiO<sub>2</sub> was dispersed in 20 mL deionized H<sub>2</sub>O and 40 mL ethanol dissolved with 0.13 g Ba(OH)<sub>2</sub> under vigorously stirring. The resultant mixture was transferred into 100 mL Teflon-lined autoclave, sealed and maintained at 160 °C for 12 h. The resultant product was then rinsed with dilute acid solution to remove the coexisted BaCO<sub>3</sub> impurity possibly formed during the hydrothermal process, followed by rinsing with copious deionized water and finally dried at 60 °C in air.

**Synthesis of pure BaTiO<sub>3</sub>.** 0.1 g porous TiO<sub>2</sub> was dispersed in 20 mL deionized H<sub>2</sub>O and 40 mL ethanol dissolved with 1.183 g Ba(OH)<sub>2</sub>•8H<sub>2</sub>O under vigorously stirring for 30 min. The resultant mixture was transferred into 100 mL Teflon-lined autoclave, sealed and maintained at 100 °C for 12 h. The resultant product was then rinsed with dilute acid solution to remove the coexisted BaCO<sub>3</sub> impurity possibly formed during the hydrothermal process, followed by rinsing with copious deionized water and finally dried at 60 °C in air.

**Fabrication of TiO<sub>2</sub>/BaTiO<sub>3</sub>-S or TiO<sub>2</sub>-S or BaTiO<sub>3</sub>-S composite cathodes.** The sulfur species were loaded onto the TiO<sub>2</sub>/BaTiO<sub>3</sub> (or TiO<sub>2</sub> or BaTiO<sub>3</sub>) by a conventional melt-diffusion process. In a typical procedure, sulfur and TiO<sub>2</sub>/BaTiO<sub>3</sub> (or TiO<sub>2</sub> or BaTiO<sub>3</sub>) powders with a mass ratio of 6:4 were thoroughly mixed, followed by transferred into 25 mL Teflon-lined autoclave filled with ultrapure Ar, sealed and heated at 155 °C for 12 h. Then, the autoclave was cooled naturally to room temperature.

### **Materials characterization.**

Powder X-ray diffraction patterns (XRD) were recorded on a Bruker diffractometer with Cu K $\alpha$  radiation ( $\lambda=0.154056$  nm). The morphology of the samples was observed by a scanning electron microscope (SEM, Hitachi S-4800) attached with an energy-dispersive X-ray (EDX) spectrometer. Transmission electron microscopy (TEM) and high-resolution transmission electron microscopy (HRTEM) micrographs were acquired on a JEOL JEM-2100F microscope. Brunner-Emmett-Teller (BET) specific

surface area and Barrett-Joyner-Halenda (BJH) pore size distribution were determined by nitrogen isotherms measured at 77 K on a Tri Star II 3020 surface area and porosity analyzer. Prior to sorption tests, the samples were degassed at 100 °C for 48 h in a vacuum line.

### **Visual adsorption experiments of polysulfides.**

Li<sub>2</sub>S<sub>6</sub> solution (0.5 mM) was made by dissolution of sulfur and Li<sub>2</sub>S with molar ratio of 5:1 in DOL/DME (V/V 1:1) in an Ar-purged glovebox. The resulting solution was continuously stirred for 24 h at 50 °C to prepare a stock solution. For visual adsorption experiments, 20 mg of active materials were respectively added into 2 mL 0.5 mM Li<sub>2</sub>S<sub>6</sub> solution and kept static for 1 h.

### **Electrochemical measurements.**

The electrochemical tests were carried out using CR2025 coin cells with lithium foils as counter and reference electrodes, and microporous membrane (Celgard 2400) as separator. The working electrodes were fabricated by mixing the active materials (TiO<sub>2</sub>/BaTiO<sub>3</sub>-S, TiO<sub>2</sub>-S or BaTiO<sub>3</sub>-S), acetylene black, and polyvinylidene fluoride (PVDF) binder with a mass ratio of 8:1:1 in N-methyl-2-pyrrolidone (NMP) to form a slurry. The slurry was uniformly coated on aluminum foils and dried at 55 °C for 12 h in vacuum and then cut into circular disks with an average loading of ~1.2 mg/cm<sup>2</sup>. The electrolyte was 1.0 M solution of lithium bis(trifluoromethanesulfonyl)imide (LiTFSI) with 1wt% LiNO<sub>3</sub> dissolved in 1,3-dioxolane (DOL) and 1,2-dimethoxy ethane (DME)

(1:1, v/v) with a ratio of electrolyte/sulfur fixing at  $\sim 10$  mL/g. The coin cells were assembled in an argon-purged glovebox with both moisture and oxygen contents below 0.3 ppm. Cyclic voltammetry (CV) curves were recorded on an electrochemical workstation (CHI 604e) within a potential region of 1.8~2.8 V vs. Li<sup>+</sup>/Li at 0.2 mV/s. Galvanostatic discharge/charge profiles were conducted using a LAND-CT2001A at different current densities. All the electrochemical tests were carried out at room temperature.

### **CV tests using symmetrical electrodes.**

The Li-S cells for symmetric CV measurements were prepared by using the two same electrode made of same active materials (TiO<sub>2</sub>, BaTiO<sub>3</sub> or TiO<sub>2</sub>/BaTiO<sub>3</sub>). An Li<sub>2</sub>S<sub>6</sub> electrolyte solution (0.2 M) was made by dissolving Li<sub>2</sub>S and sulfur powders with a molar ratio of 1:5 in DOL/DME (V/V 1:1). The electrodes were fabricated by blending active materials and PVDF binder with a weight ratio of 4:1 in NMP to form a slurry. Then the resulting slurry was coated on Al foils and dried for 12 h at 70 °C in vacuum, followed by cutting into circular disks. The CV measurements were carried out at 2 mV/s.

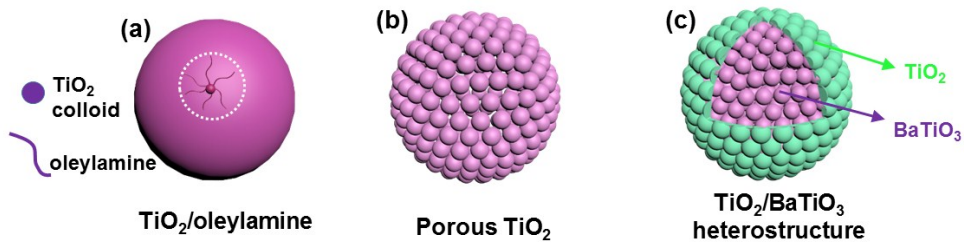


Fig. S1. Schematic of synthesis procedure of porous coherent TiO<sub>2</sub>/BaTiO<sub>3</sub> nanocomposite as a cathode host for lithium-sulfur batteries.

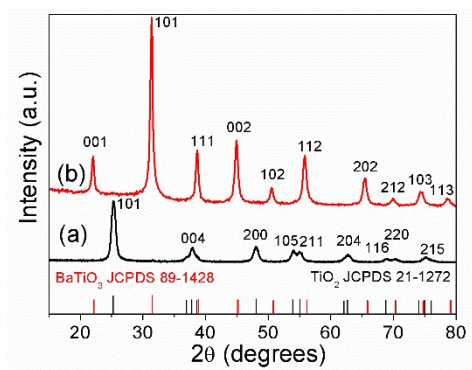


Fig. S2. XRD patterns of (a) porous  $\text{TiO}_2$  sample prepared by hydrothermal reaction and (b) pure  $\text{BaTiO}_3$ .

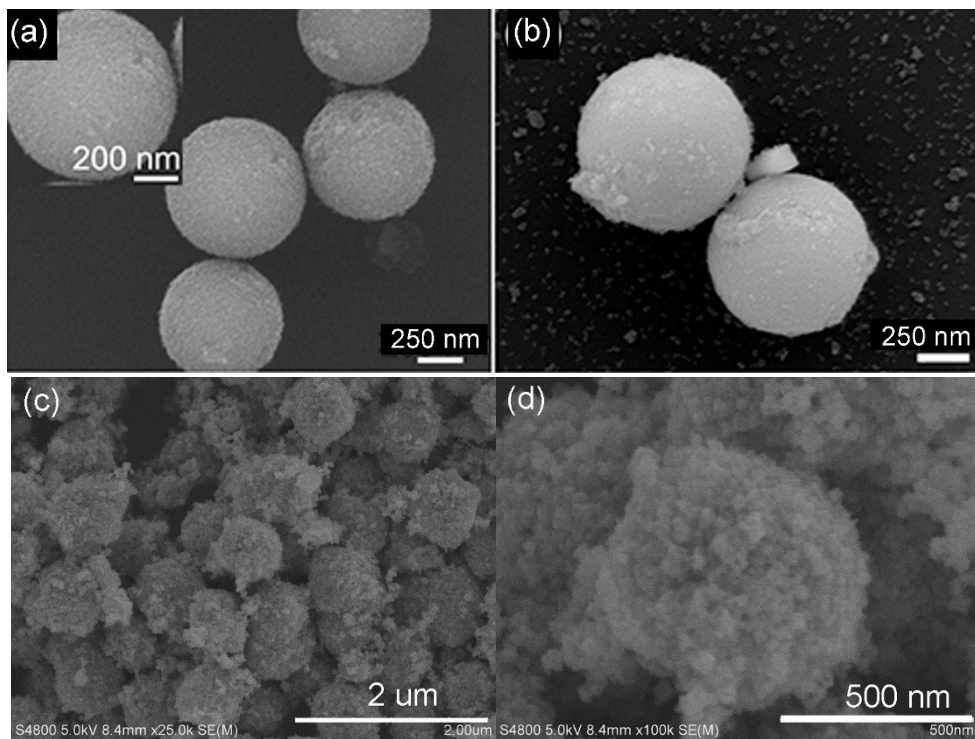


Fig. S3. SEM images of (a) porous  $\text{TiO}_2$ , (b)  $\text{TiO}_2/\text{BaTiO}_3$  composite spheres, and (c, d) of pure  $\text{BaTiO}_3$ .

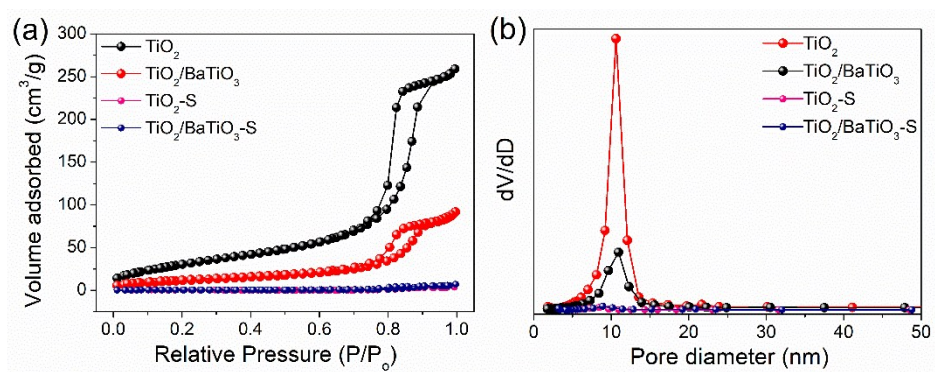


Fig. S4. (a) Nitrogen adsorption/desorption isotherms and (b) pore size distribution plots of  $\text{TiO}_2$ ,  $\text{TiO}_2/\text{BaTiO}_3$ ,  $\text{TiO}_2\text{-S}$  and  $\text{TiO}_2/\text{BaTiO}_3\text{-S}$  samples.

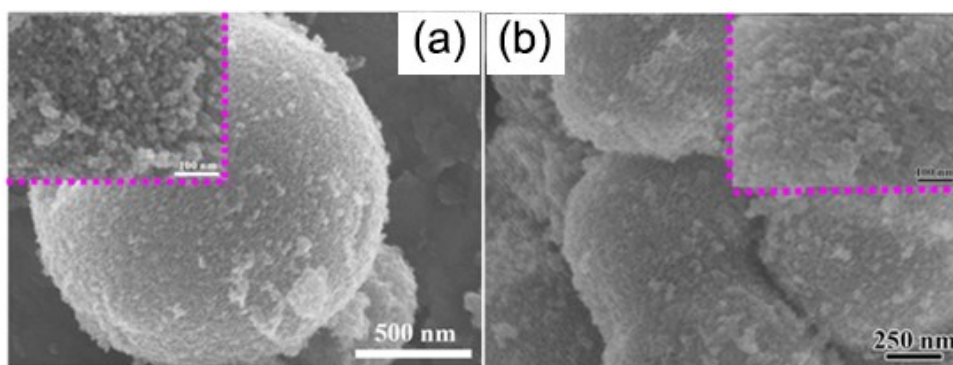


Fig. S5. SEM images of (a)  $\text{TiO}_2$ -S and (b)  $\text{TiO}_2/\text{BaTiO}_3$ -S composite samples.

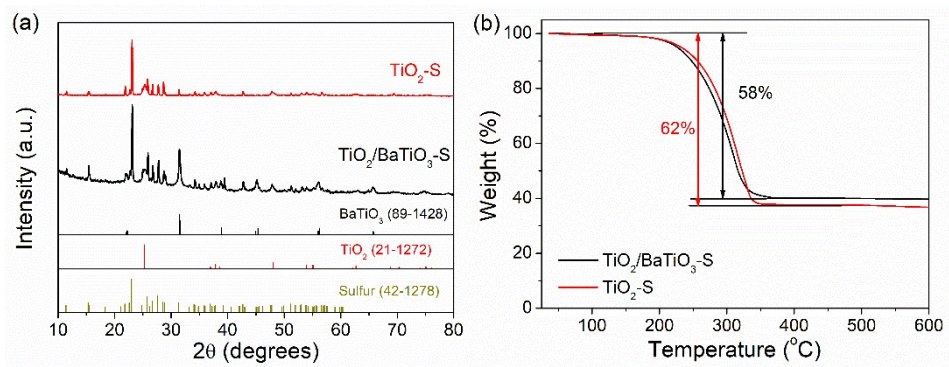


Fig. S6. (a) XRD patterns, (b) TGA curves of  $\text{TiO}_2/\text{BaTiO}_3\text{-S}$  and  $\text{TiO}_2\text{-S}$  samples.

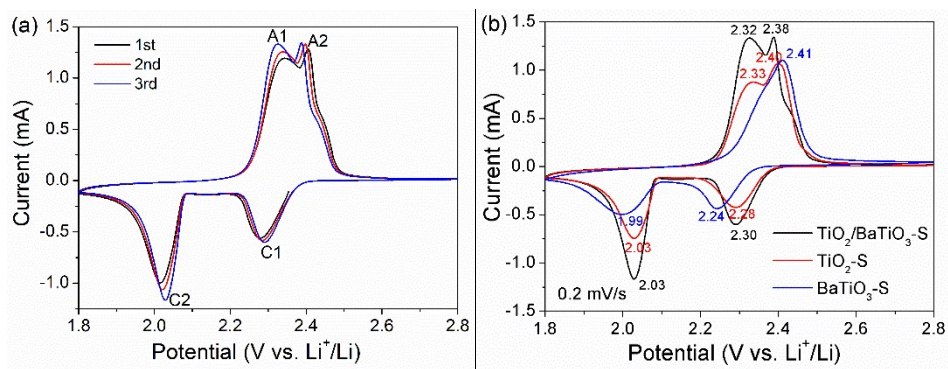


Fig. S7. Cyclic voltammetry curves of (a) TiO<sub>2</sub>/BaTiO<sub>3</sub>-S for the first 3 cycles and (b) 3<sup>rd</sup> cycle of the 3 electrodes at 0.2 mV/s.

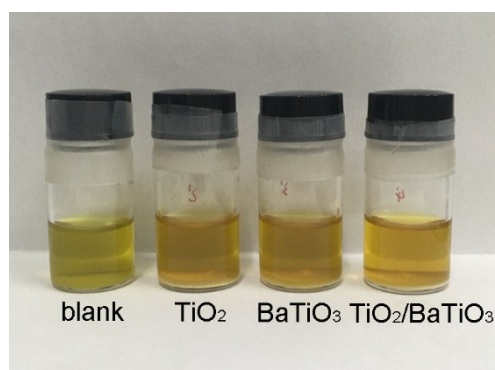


Fig. S8. Digital photos of vials with  $\text{TiO}_2$ ,  $\text{BaTiO}_3$  and  $\text{TiO}_2/\text{BaTiO}_3$  (20 mg each), respectively, soaked in 2 mL 0.5 mM  $\text{Li}_2\text{S}_6$  solution in DOL/DME (V/V 1:1) after 1 h.

Fig. S8 shows that the  $\text{Li}_2\text{S}_6$  solution turned from yellow-green to yellow after adding the active materials. The remaining yellow color suggests that the  $\text{Li}_2\text{S}_6$  has not been fully adsorbed on the active material surface within the short period possibly due to the relatively low specific surface area of these materials. Nonetheless, the  $\text{TiO}_2/\text{BaTiO}_3$  shows a shallower yellow color than that of its  $\text{TiO}_2$  and  $\text{BaTiO}_3$  counterparts. In addition, the specific surface area of  $\text{TiO}_2/\text{BaTiO}_3$  ( $43 \text{ m}^2/\text{g}$ ) is about 1/3 of that of  $\text{TiO}_2$  ( $121 \text{ m}^2/\text{g}$ ). These results suggest that  $\text{TiO}_2/\text{BaTiO}_3$  possess higher adsorption ability towards polysulfide than the other two hosts.

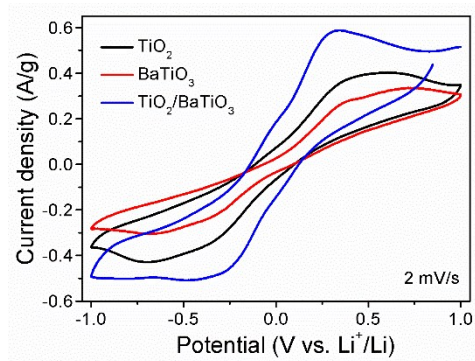


Fig. S9. CV of symmetric Li-S cells with identical  $\text{TiO}_2$ ,  $\text{BaTiO}_3$  and  $\text{TiO}_2/\text{BaTiO}_3$  electrodes, respectively, in 0.2 M  $\text{Li}_2\text{S}_6$  electrolytes at 2 mV/s.

From Fig. S9, it is evident that the Li-S cell using two symmetric  $\text{TiO}_2/\text{BaTiO}_3$  electrodes exhibits the fastest and largest current response during both cathodic and anodic processes among the three Li-S cells, suggesting its fastest reaction kinetics.

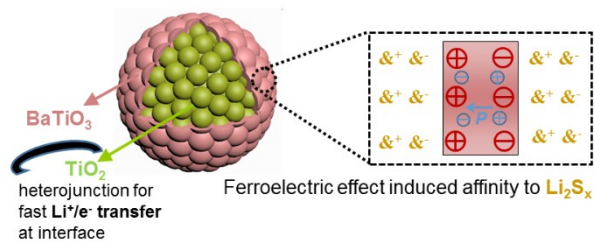


Fig. S10. Schematic structure merits of the  $\text{TiO}_2/\text{BaTiO}_3$  heterostructure as cathode host for Li-S batteries.

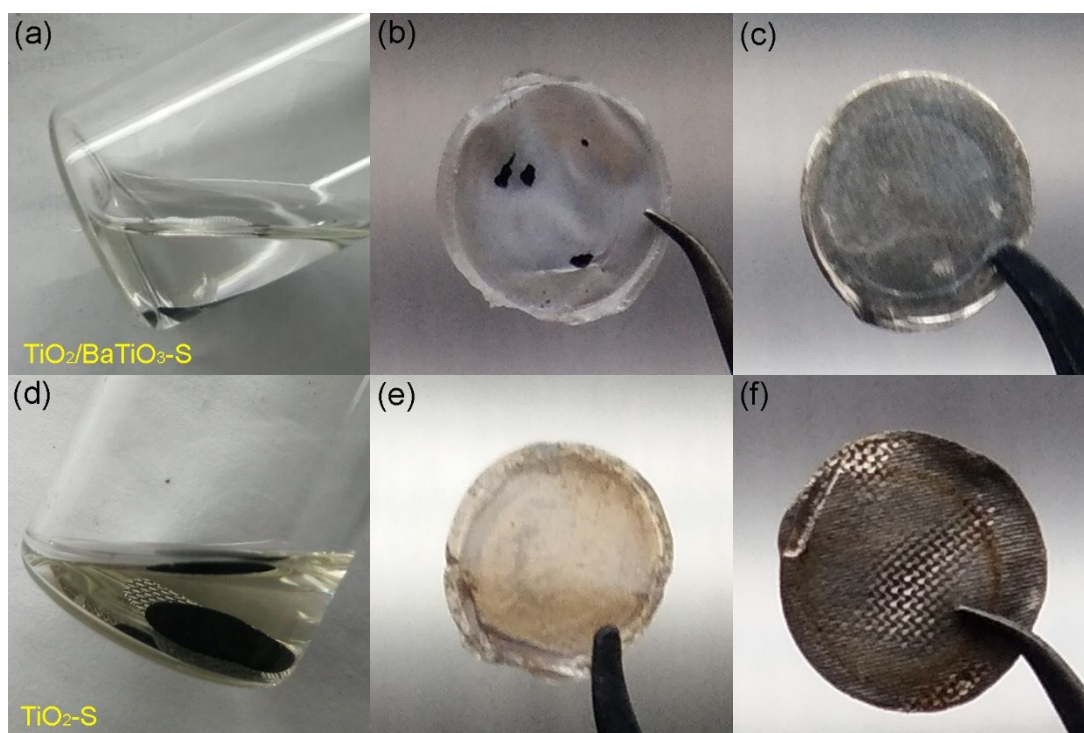


Fig. S11. Digital photos of the cathodes soaked in electrolytes (a, d), Celgard separators (b, e) and lithium anodes (c, f) taken from electrochemically cycled Li-S cells with  $\text{TiO}_2/\text{BaTiO}_3\text{-S}$  cathode (a-c) and  $\text{TiO}_2\text{-S}$  cathode (d-f), respectively, suggesting the stronger confinement of  $\text{TiO}_2/\text{BaTiO}_3$  for polysulfides.

**Table S1.** Comparison of rate capability of our TiO<sub>2</sub>/BaTiO<sub>3</sub>-S cathode with those reported in recent literature.

<b>Cathode</b>	<b>Capacity (mAh/g) at 0.5 C</b>	<b>Capacity (mAh/g) at 1 C</b>	<b>Capacity (mAh/g) at 2 C</b>	<b>Capacity (mAh/g) at 5 C</b>	<b>Reference</b>
<b>TiO<sub>2</sub>/BaTiO<sub>3</sub> junction</b>	<b>842</b>	<b>704</b>	<b>607</b>	<b>493</b>	<b>This work</b>
Hierarchical TiO <sub>2</sub>	NA	740	640	490	[1]
Hollow TiO <sub>2</sub>	800	630	560	NA	[2]
TiO <sub>2</sub> -graphene	710	600	480	NA	[3]
BaTiO <sub>3</sub> nanoparticles	800	700	610	440	[4]

NA: not available

**Table S2.** Comparison of cycling performance of our TiO<sub>2</sub>/BaTiO<sub>3</sub>-S cathode with those reported in recent literature.

<b>Cathode</b>	<b>Current density (C)</b>	<b>Cycle number</b>	<b>Initial capacity (mAh/g)</b>	<b>Retained Capacity (mAh/g)</b>	<b>Retention ratio (%)</b>	<b>Reference</b>
<b>TiO<sub>2</sub>/BaTiO<sub>3</sub> junction</b>	<b>0.5</b>	<b>500 (334)</b>	<b>898</b>	<b>541 (624)</b>	<b>60 (69.5)</b>	<b>This work</b>
<b>Porous TiO<sub>2</sub></b>	<b>0.5</b>	<b>334</b>	<b>880</b>	<b>555</b>	<b>63</b>	<b>This work</b>
<b>CNT</b>	<b>0.5</b>	<b>500</b>	<b>881</b>	<b>466</b>	<b>52.9</b>	<b>This work</b>
Hollow TiO <sub>2</sub>	0.5	300	850	520	61	[2]
NG/SnS <sub>2</sub> /TiO <sub>2</sub>	0.5	500	900	572	63.5	[5]
TiO <sub>2</sub> nanotubes/rGO	0.5	200	1200	630	52.5	[6]
TiO <sub>2</sub> nanowire array	0.5	100	800	525	65.6	[7]
Mesoporous TiO <sub>2</sub> tubes	1	500	850	400	47	[8]
PEDOT coated TiO <sub>2</sub>	1	500	900	530	58.9	[9]

## References

1. L. Gao, M. Cao, Y. Q. Fu, Z. Zhong, Y. Shen and M. Wang, *J. Mater. Chem. A*, 2016, **4**, 16454-16461.
2. M. Fang, Z. Chen, Y. Liu, J. Quan, C. Yang, L. Zhu, Q. Xu and Q. Xu, *J. Mater. Chem. A*, 2018, **6**, 1630-1638.
3. T. Zhou, W. Lv, J. Li, G. Zhou, Y. Zhao, S. Fan, B. Liu, B. Li, F. Kang and Q.-H. Yang, *Energy Environ. Sci.*, 2017, **10**, 1694-1703.
4. K. Xie, Y. You, K. Yuan, W. Lu, K. Zhang, F. Xu, M. Ye, S. Ke, C. Shen, X. Zeng, X. Fan and B. Wei, *Adv. Mater.*, 2017, **29**, 1604724.
5. X. Li, G. Guo, N. Qin, Z. Deng, Z. Lu, D. Shen, X. Zhao, Y. Li, B.-L. Su and H.-E. Wang, *Nanoscale*, 2018, **10**, 15505-15512.
6. J. Song, J. Zheng, S. Feng, C. Zhu, S. Fu, W. Zhao, D. Du and Y. Lin, *Carbon*, 2018, **128**, 63-69.
7. Y. Yan, T. Lei, Y. Jiao, C. Wu and J. Xiong, *Electrochim. Acta*, 2018, **264**, 20-25.
8. X. Qian, X. Yang, L. Jin, D. Rao, S. Yao, X. Shen, K. Xiao, S. Qin and J. Xiang, *Mater. Res. Bull.*, 2017, **95**, 402-408.
9. K. Luan, S. Yao, Y. Zhang, R. Zhuang, J. Xiang, X. Shen, T. Li, K. Xiao and S. Qin, *Electrochim. Acta*, 2017, **252**, 461-469.